Effect of Saturation Third Harmonic on the Performance of Squirrel-Cage Induction Machines

Yuefeng Liao, Thomas A. Lipo

Department of Electrical and Computer Engineering
University of Wisconsin-Madison
1415 Johnson Drive
Madison, WI 53706, U.S.A.

ABSTRACT: This paper contributes to the understanding of the behavior of the saturation third harmonic and how energy is converted from fundamental to third harmonic form in a squirrel-cage induction machine in the presence of magnetic saturation. It is shown that the power transferred via the third harmonic airgap flux is accounted for by a change in the magnitude and phase-shift in the fundamental airgap flux. A procedure is proposed to link the rotor third harmonic circuit quantities to a set of equivalent fundamental component circuit quantities which leads to a modified equivalent circuit for the induction machine.

1. Introduction

Magnetic saturation is an inevitable operating feature in almost all electromagnetic devices. For the case of induction machines, all practical designs place the induction machine under slightly to moderately saturated conditions during normal operation. Moreover, from the perspective of control, it is sometimes desirable to push the motor in an adjustable speed drive system into the highly saturated region to achieve temporary increased torque output, increased efficiency or other performance gains [1-2]. The promise of performance gains in adjustable speed drives makes it particularly desirable to understand in detail how the motor will behave under saturated conditions.

Among other phenomena, saturation causes a special type of spatial harmonic, termed saturation harmonics, which are very different from the time harmonics due to solid state power supplies and the spatial harmonics due to non-ideal winding distribution and slotting. Although the effects of the latter on the performance of the squirrel-cage induction machine have been well explored and understood, the same can by no means be said of the harmonics due to saturation of the main flux path despite a number of research efforts spanning several decades [3,4].

One important fact concerning saturation harmonics is that they all travel with the same rotational speed in the airgap as does the fundamental. Consequently, all rotor induced saturation harmonic currents have the same slip and therefore participate in energy conversion, i.e. producing useful torque. Therefore, the motor can be viewed as a cascaded combination of many sub-motors working under different saturation harmonics. This feature is absent from other types of harmonics for which the slip is high and the induced rotor current has essentially a reactive component only.

For the 5th, 7th and other non-triplen saturation harmonics, the stator windings, being Y-connected and fed by a voltage source, present a low impedance circuit to dampen the effect of the corresponding airgap flux, an action similar to that of the rotor currents for other types of harmonics. Therefore, the resultant harmonic field in the airgap is small due to this interaction. However, for the third harmonic, no stator current can possibly exist to counteract the time rate of change of the airgap flux. As a result, rotor currents flow which are not damped out by corresponding stator currents and will produce substantial torque. It

will be shown in the next section that the presence of the third harmonic MMF due to induced rotor third harmonic currents distorts the magnetizing MMF distribution in the airgap, and saturation in the teeth causes re-distribution of the spectrum of the airgap flux density waveform. Therefore, the magnitude and the phase-shift of the fundamental is changed, resulting in torque production despite the absence of third harmonic current in the stator windings, as was pointed out by Lee [3]. It should be noted that with current regulation, the stator windings do not allow any current flows due to saturation harmonics. Thus the induced rotor currents will contain the 5th, 7th and other non-triplen harmonics in addition to the third harmonic. However, the effect due to the third harmonic will still dominate because the magnitude of the higher saturation harmonics are lower.

Recently, a paper was presented which outlined an approach for dynamic modelling of the saturated induction motor by the use of a pseudo variable airgap length [5]. Although this approach succeeds in modeling the fundamental and the third harmonic voltages, especially for small motors with moderate saturation, the method is still based upon superposition and the assumption of negligible third harmonic rotor current. Thus, it appears that the very nature of the main flux path saturation and the role in the process of energy conversion by the third harmonic remains obscured.

It is clear that the principle of superposition should be used with great caution in the presence of nonlinearity. Numerous papers have been published addressing the issue of saturation modeling in induction motors as illustrated by Refs. 6-9. However, these investigations are all limited to the fundamental component only. The fact of power transfer via harmonic/fundamental interaction in the presence of saturation, as was pointed out by Lee [3], has been largely ignored in these more recent papers.

It is the objective of this paper to investigate in detail the effect of saturation on the performance of squirrel-cage induction machines. First, the basic physics of the saturation phenomena is reviewed; Next, by using a simplified airgap field model similar to that used by Chalmers and Dodgson, the airgap flux density distribution and saturation characteristics are obtained numerically. The variation of the third harmonic as the load changes is then characterized and the peculiarity of the change in the fundamental flux density with load is demonstrated. Based on this analysis, an important parameter, the third harmonic magnetizing inductance is introduced as a circuit parameter. Finally, a modified equivalent circuit including the third harmonic is proposed which is believed to hold promise for improved performance calculation and dynamic control of induction machines using field orientation.

2. Basic Physics of Power Transfer via Third Harmonic

It is well recognized that the torques produced by an induction motor to various harmonic components in the airgap magnetic field can be superimposed despite the nonlinearity of the magnetic flux path. Assume that there exists a certain airgap flux density waveform consisting of fundamental and the third harmonic only, i.e.,

$$B(\theta_r) = B_{1m} \sin(\theta_r) + B_{3m} \sin(3\theta_r + \alpha) \tag{1}$$

The torque expressions for the fundamental and the third harmonic can then be written as:

$$T_{e1} = (\frac{p}{2}) \frac{1}{2\sqrt{2}} m_r \Phi_{1m} I_{1rb} \cos\varphi_{1r} \tag{2}$$

$$T_{e3} = 3(\frac{p}{2}) \frac{1}{2\sqrt{2}} m_r \Phi_{3m} I_{3rb} \cos\varphi_{3r} \tag{3}$$

where

$$\Phi_{jm} = \frac{2B_{jm} D_i l_{eff}}{jp} \qquad j=1,3 \tag{4}$$

$$I_{1rb} = \frac{E_{1r}}{| R_r + jS_1\omega_e L_{1r} |} = \frac{\frac{1}{2\sqrt{2}} S\omega_e \Phi_{1m}}{\sqrt{R_r{}^2 + (S\omega_e L_{1r})^2}} \tag{5}$$

$$I_{3rb} = \frac{E_{3r}}{| R_r + jS_3 3\omega_e L_{1r} |} = \frac{\frac{1}{2\sqrt{2}} 3S\omega_e \Phi_{3m}}{\sqrt{R_r{}^2 + (3S\omega_e L_{1r})^2}} \tag{6}$$

$$\cos \varphi_{1r} = \frac{R_r}{\sqrt{R_r{}^2 + (S\omega_e L_{1r})^2}} \tag{7}$$

$$\cos \varphi_{3r} = \frac{R_r}{\sqrt{R_r{}^2 + (3S\omega_e L_{1r})^2}} \tag{8}$$

I_{1rb} , I_{3rb} are the rotor bar currents, and m_r is the number of rotor bars per pole pair.

The ratio of the third harmonic torque to the fundamental torque can be established as

$$\tau = \frac{T_{e3}}{T_{e1}} = (\frac{3\Phi_{3m}}{\Phi_{1m}})^2 \frac{R_r{}^2 + (S\omega_e L_{1r})^2}{R_r{}^2 + (3S\omega_e L_{1r})^2} \cong (\frac{B_{3m}}{B_{1m}})^2 \tag{9}$$

It is clear from Eqn. (9) that the torque produced by the third harmonic is only significant for the case of deep saturation where the ratio of B_{3m} to B_{1m} tends to the value of limit of 1/3. In this extreme case, the torque produced by the third harmonic of flux density would be about 10% of the rated torque. Note also that the third harmonic current would be about 1/3 of the rated current, but the associated copper loss associated would be only 10% of the rated rotor copper losses.

In the above discussion, the torque produced by the third harmonic was obtained from the rotor side. Questions may be raised as to how this energy transfer is reflected on the stator side where there exists only a fundamental current component. To answer to this quandary it is useful to examine an extreme case where the stator windings are injected with only a magnetizing component and the airgap third harmonic MMF due to the rotor third harmonic current is phase-shifted from the fundamental MMF by an angle γ. The resultant airgap MMF would then consist of two components, i.e.

$$F(\theta_r) = F_{1m}\sin(\theta_r) + F_{3m}\sin(3\theta_r + \gamma) \tag{10}$$

To examine the saturation effect of the teeth, the MMF drops in the airgap and the stator and rotor cores will be initially neglected. The airgap flux density waveforms can then be obtained graphically, as shown in Fig. 1. The saturation curve of the iron is also shown in the figure. In Fig. 1a, the airgap flux density waveform is symmetrical, flat-topped when the airgap MMF is sinusoidal. The third harmonic airgap flux density

component is found to be in-phase with the fundamental. This conclusion can be extended to the case when a third harmonic MMF of same or opposite polarity is added to the fundamental MMF.

When the phase of the third harmonic MMF is shifted by some angle γ due to induced rotor 3rd harmonic current, the resultant airgap MMF waveform will no longer be symmetrical. As can be seen in Fig. 1b, the presence of the third harmonic MMF due to induced rotor third harmonic current distorts the magnetizing MMF distribution in the airgap. Therefore, saturation in the teeth will exert a rotor angle dependent "flattening" effect on the flux density distribution, causing a re-distribution of the spectrum of the airgap flux density waveform. As a result, the phase, as well as the magnitude of the fundamental flux is changed, causing a torque production component in the fundamental stator current and resulting in torque production despite the absence of a third harmonic current in the stator windings.

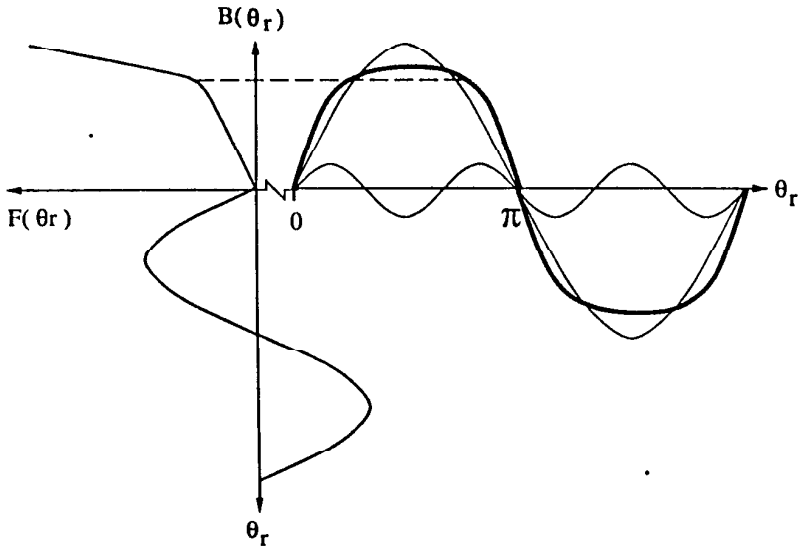

(a) Fundamental MMF only

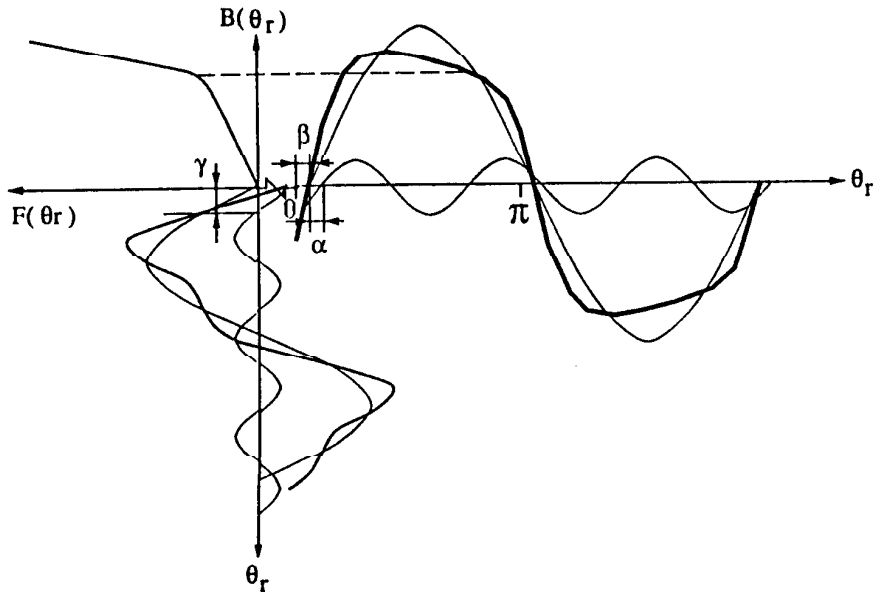

(b) With third harmonic MMF

Fig. 1 Airgap Flux Density Waveforms with Different Excitations

Thus far it has been assumed that the resultant third harmonic flux in the airgap is known. In reality, the determination of the resultant third harmonic flux is very complicated due to the fact that, like Y/Δ connected 3-phase transformers, it allows a co-existence of the third harmonic voltage (on the stator side) and the third harmonic current (on the rotor side). The procedure for solving the problem involves first assuming a certain rotor current, solving for the third harmonic flux for a given stator and rotor MMF distribution by field analysis, then iteratively solving for the rotor current. However, as will be shown in Section 5, a third harmonic magnetizing inductance can be introduced to represent the interaction of the rotor third harmonic current to the third harmonic airgap flux caused by the stator fundamental current, thus making the problem of determining the third harmonic flux considerably simplified.

3. Quasi- 2-D Modeling of the Airgap Field

A simplified field model similar to that used by Chalmers and Dodgson is used here for the purpose of predicting the airgap flux density distribution in the bore of the induction machine in the presence of tooth saturation. This quasi- two dimensional field model is based on the following assumptions:

(1) the stator and rotor currents are sinusoidal and symmetrical, as is the case when the motor is fed from utilities or CRPWM (current regulated PWM) inverters;

(2) the stator and rotor windings are sinusoidally distributed, which is a good approximation of modern poly-phase induction machines;

(3) the number of stator slots and rotor slots are sufficiently large so that the space harmonics due to slotting are negligible.

The no-load condition is the simplest case where no rotor current exists. The stator current can be replaced by an airgap current sheet which is sinusoidally distributed, as shown in Fig. 2.

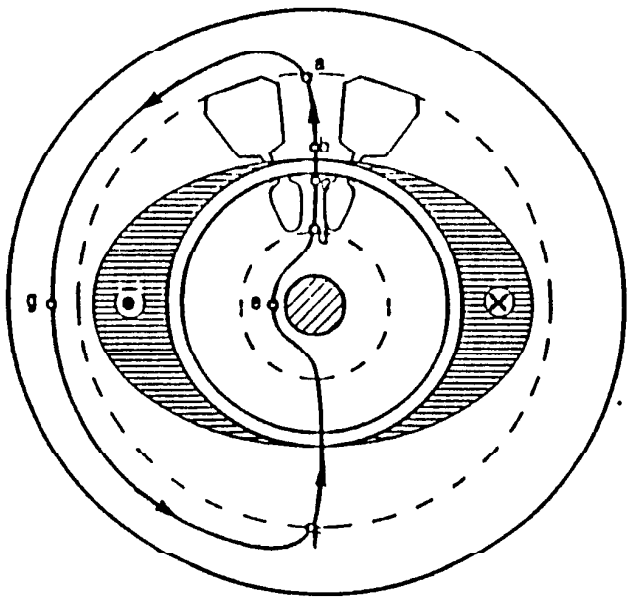

Fig. 2 Quasi 2-D Field Model for Induction Machines

The airgap flux density at a specific rotor angle $B(\theta_r)$ can be solved by applying Ampere's Law along the path as shown in Fig. 2.

$$F(\theta_r) = \frac{1}{2}\int_0^{\theta_r} f(\xi)d\xi$$

$$= MMF_{ab} + MMF_{bc} + MMF_{cd} + MMF_{de} + MMF_{ag} \qquad (11)$$

In the above equation, the MMF drops in the air-gap MMF_{bc}, the stator and rotor teeth MMF_{ab} and MMF_{cd} are all known functions of $B(\theta_r)$. The only unknown in the equation is the core flux density distribution. However, for most practical designs, the core is only slightly saturated and is thus not very critical to the spectral distribution of the airgap flux density. Therefore, it can be accounted for *a priori*. More accurately, Chalmers and Dodgson's iterative updating method can be utilized [4]. However, it can be noted that Eqn. (11) is nonlinear with respect to $B(\theta_r)$ for given $F(\theta_r)$. The following procedures are followd:

Step I: A saturation curve relating the MMF required to the airgap flux density produced is obtained by taking values of B and computing the MMF drops across the airgap, stator and rotor teeth as per Eqn. (11).

Step II: The saturation curve is spline interpolated to find the airgap flux density distribution $B(\theta_r)$ for a given $F(\theta_r)$ with suitable allowance for the MMF drops in the stator and rotor cores.

Step III: A Fast Fourier Transform is then used to find the magnitudes and phase-shifts of the harmonics of the airgap flux density distribution.

The problem is reduced to that of a one dimensional problem with nonlinear coefficients. The solution of $B(\theta_r)$ can thus be obtained very efficiently.

When the motor is loaded, the stator current will have an additional working component in addition to the magnetizing component. Rotor currents, both fundamental and the third harmonic, are induced and the picture becomes very complicated. However, the MMF due to an induced fundamental rotor current will cancel that due to the working component of the stator current. As a result, the airgap MMF distribution is about the same as that of the no-load condition. The difference from that of the no-load flux distribution is only a biasing of leakage flux. These leakage fluxes are normally very small and moreover, the orientation of these leakage flux fields are right angles with that of the fundamental airgap field. Therefore, the existence of this leakage biasing will not seriously affect the saturation situation in the teeth.

As for the induced rotor third harmonic current, it will ideally form a sinusoidal MMF sheet in the airgap (again neglecting slotting effects). Therefore, the resultant airgap MMF distribution under a loaded condition would consist of the fundamental MMF sheet and the third harmonic MMF sheet, i.e.

$$F(\theta_r) = F_{1m}\sin\theta_r + F_{3m}\sin(3\theta_r + \gamma) \qquad (12)$$

The approach proposed for the no-load condition can now be applied to find the airgap flux distribution.

4. Calculated Airgap Flux Density and Saturation Characteristics of the Studied Machine

The quasi-2 dimensional model for the airgap field is used to investigate the airgap flux distribution and saturation characteristics of a 25 horsepower induction motor as studied by Lee and Chalmers and Dodgson [3,4]. Nameplate values and parameters of the motor are listed in Appendix I. The calculated saturation curves for the fundamental and the third harmonic airgap flux at no-load are shown in Fig. 2. It can be seen that at rated flux level, the third harmonic flux density is only 10%. When the magnetizing current is doubled, the third harmonic is increased by a factor of 2.6 while the fundamental is up by 20% only.

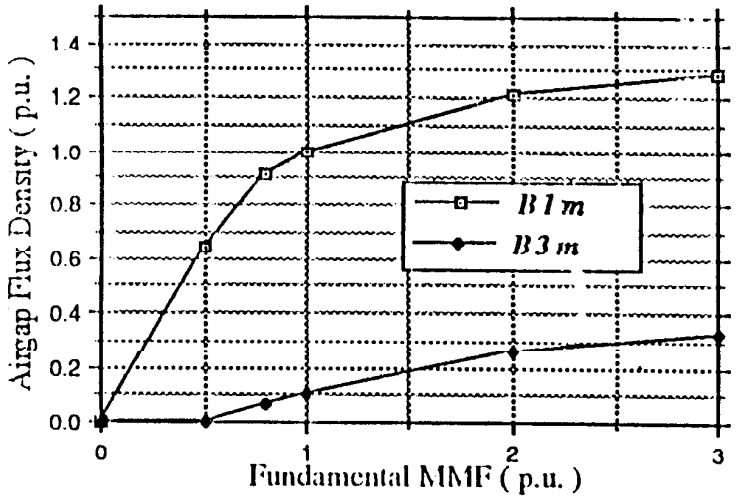

Fig. 3 Saturation Curves for the Fundamental and the Third Harmonic Airgap Flux Density at No-Load

Next, the magnetizing or demagnetizing effects of the third harmonic rotor current at different flux levels are investigated. The flux levels chosen are those corresponding to 1.0, 2.0 and 3.0 times the rated fundamental MMF excitation. The magnitude of the third harmonic MMF is chosen up to 0.5 times the rated fundamental MMF, which is a rather wide range of value even for large machines with X_m = 5.0 p.u.

Firstly, an in-phase third harmonic MMF is added to the airgap fundamental MMF. The changes in the magnitudes of the fundamental and the third harmonic are shown in Fig. 4. It can be seen that the curves in Fig. 4b, especially in the de-magnetizing region, can be approximated by straight lines. This suggests that this effect can be approximately represented by a magnetizing inductance which is function of the fundamental flux level only. Also can be seen from Fig. 4a that the magnitude of the fundamental flux is only slightly affected by the existence of the third harmonic MMF in highly saturated region.

Secondly, the airgap fundamental MMF is combined with a third harmonic MMF with 90° offset in phase with the airgap fundamental MMF. The changes in the magnitudes of the fundamental and the third harmonic are shown in Figs. 5-6. It is very clear that the phase-shift of the fundamental flux increases continuously with the magnitude of the third harmonic MMF although the magnitude of the fundamental flux remains almost invariant. The magnitude and the phase-shift of the third harmonic flux show a more pronounced change in the presence of a third harmonic MMF.

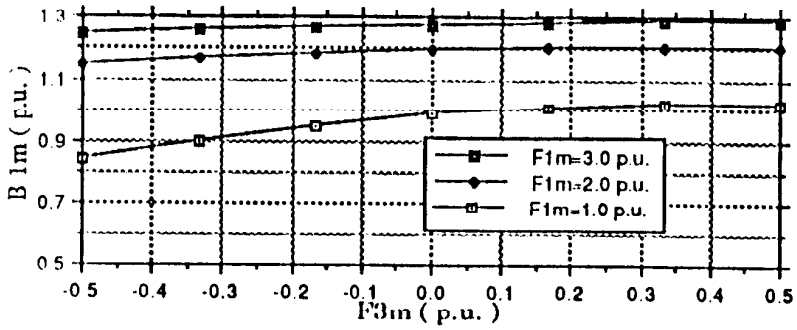

(a) Fundamental

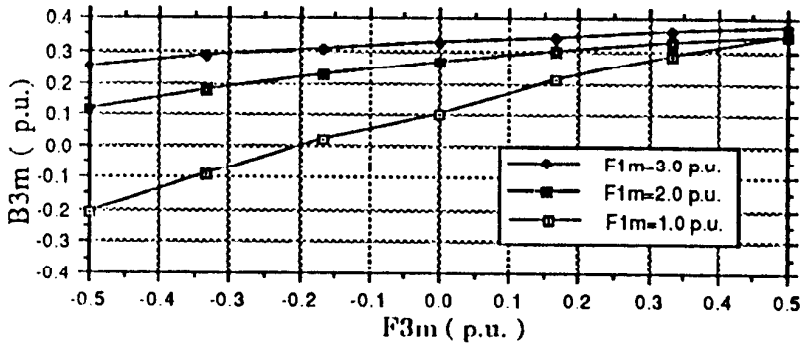

(b) 3rd harmonic

Fig. 4 Variation of the Airgap Flux Density as a Function of the d-axis 3rd Harmonic MMF

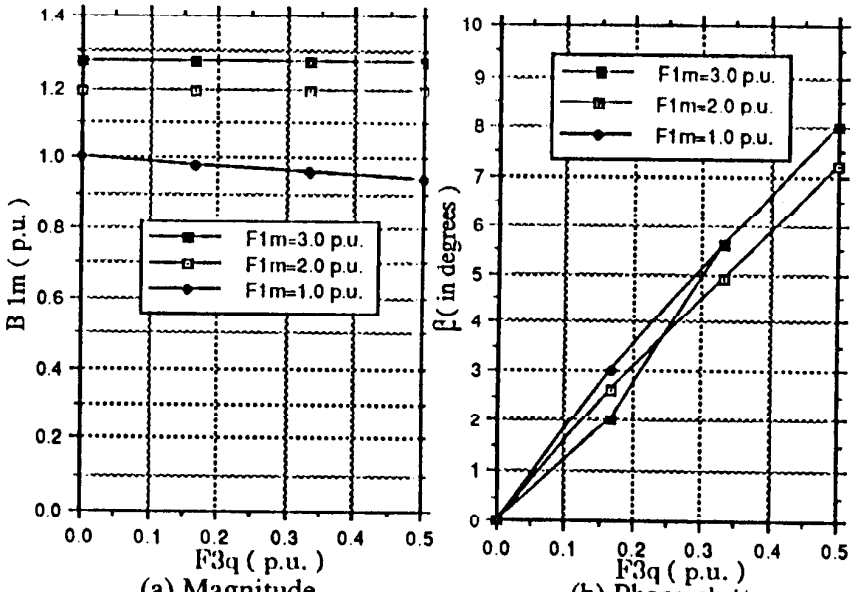

(a) Magnitude (b) Phase-shift

Fig. 5 Variation of the Airgap Fundamental Flux Density as a Function of the q-axis 3rd Harmonic MMF

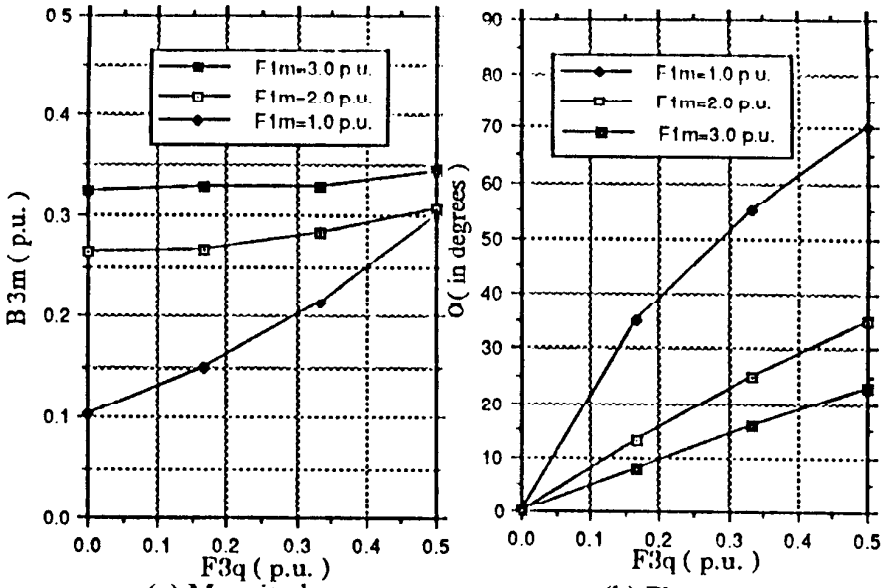

(a) Magnitude (b) Phase-shift

Fig. 6 Variation of the Airgap 3rd Harmonic Flux Density as a Function of the q-axis 3rd Harmonic MMF

Lastly, the third harmonic flux is decomposed into the d- and q- axes, as shown in Fig. 7. It is very interesting to see that the d-axis component, which is due to the fundamental MMF, remains almost unchanged while the q-axis component changes almost linearly with the applied MMF. This again suggests that this effect can be approximately represented by a magnetizing inductance which is function of the fundamental flux level only. Moreover, comparison of the slopes of the curves in Fig. 7b with that in Fig. 4b reveals an important observation that these two magnetizing inductances are almost the same. Hence, as a first approximation, the reaction of the third harmonic rotor current to the airgap third harmonic flux caused by the stator fundamental MMF can be characterized by a single magnetizing inductance which is function of the fundamental flux level only. This conclusion is not so obvious and its generalization warrants caution.

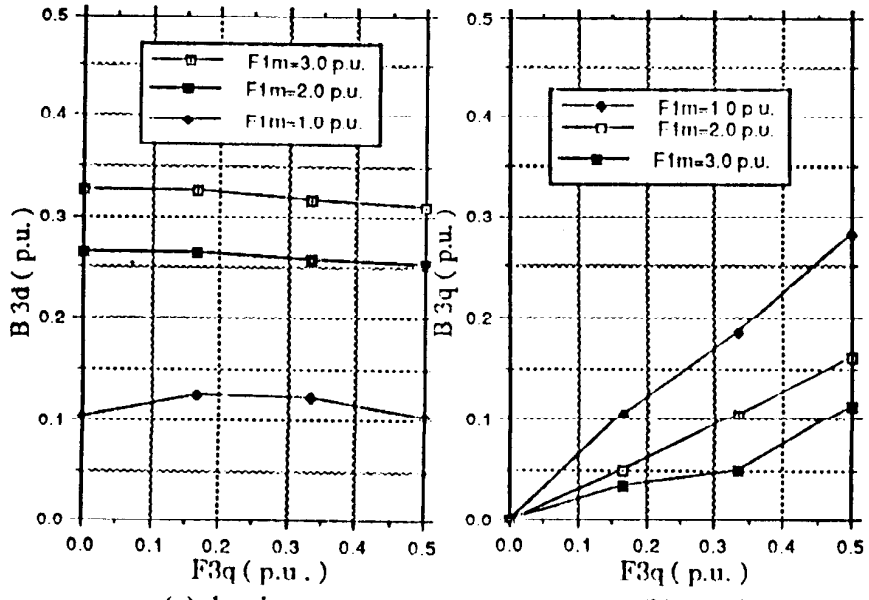

(a) d-axis (b) q-axis

Fig. 7 Variation of the d-,q-axis 3rd Harmonic Flux Density as a Function of the q-axis 3rd Harmonic MMF

5. Steady State Characteristics of Saturation Third Harmonic with Load

With the introduction of the 3rd harmonic magnetizing inductance, we are now able to use the well established space vector approach to solve for the resultant third harmonic airgap flux which is related to the torque production.

Let $\hat{\Phi}_{3s}$ represent the third harmonic airgap flux space vector due to the stator fundamental MMF, $\hat{\Phi}_{3r}$ due to the rotor third harmonic MMF, and $\hat{\Phi}_{3m}$ the resultant third harmonic airgap flux. All are peak valued vectors in the synchronous reference frame.

With the introduction of the third harmonic magnetizing inductance we will have

$$\hat{\Phi}_{3r} = I_{3r} L_{3m} \tag{13}$$

with

$$L_{3m} = \frac{\Phi_{3r}}{F_{3m}} \frac{\sqrt{2}}{2\pi} \frac{m_r}{3(\frac{p}{2})} \tag{14}$$

$$I_{3r} = \frac{E_{3r}}{R_r + j3S\omega_e L_{lr}} = \frac{j\frac{1}{2\sqrt{2}} 3S\omega_e \hat{\Phi}_{3m}}{R_r + j3S\omega_e L_{lr}} \tag{15}$$

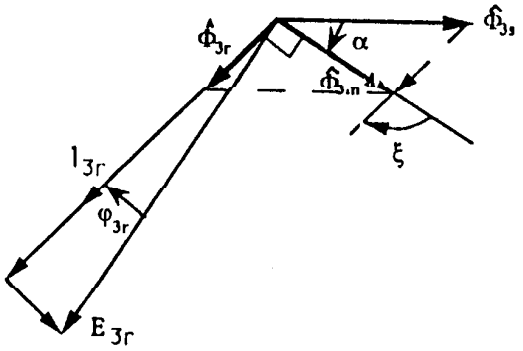

Fig. 8 Phasor Diagram for the Third Harmonic

As shown in Fig. 8, by the Law of Cosines, a quadratic equation can be formed with respect to Φ_{3m}:

$$\Phi_{3m}^2 = \Phi_{3s}^2 - \Phi_{3r}^2 + 2\,\Phi_{3s}\,\Phi_{3r}\cos\zeta \tag{16}$$

where

$$\cos\zeta = \cos(\frac{\pi}{2} + \varphi_{3r}) = -\sin\varphi_{3r} = -\frac{3S\omega_e L_{lr}}{\sqrt{R_r^2 + (3S\omega_e L_{lr})^2}} \tag{17}$$

Substituting and re-arranging, we have

$$a\Phi_{3m}^2 + b\Phi_{3s}\Phi_{3m} - \Phi_{3s}^2 = 0 \tag{18}$$

which upon solving gives

$$\Phi_{3m} = \Phi_{3s}\left(\frac{-b + \sqrt{b^2 + 4a}}{2a}\right) \tag{19}$$

with

$$a = 1 + \frac{\left(\frac{1}{2\sqrt{2}} 3S\omega_e L_{3m}\right)^2}{R_r^2 + (3S\omega_e L_{lr})^2}; \quad b = \frac{6S\omega_e L_{lr} L_{3m}}{R_r^2 + (3S\omega_e L_{lr})^2} \tag{20}$$

Note that all quantities in the above equations are actual rotor side quantities. To show the trends of $\frac{\cdot \Phi_{3m}}{\Phi_{3s}}$ as function of L_{3m}, S, R_r, L_{lr}, it is necessary to normalize the parameters on the basis of the given per unit values of machine parameters and referred to the stator side. After a lengthy derivation as shown in Appendix II, it can be found that

$$a = 1 + \frac{X_{3m}^2}{\left(\frac{r_r}{S}\right)^2 + (3X_{lr})^2}; \quad b = \frac{6X_{lr}X_{3m}}{\left(\frac{r_r}{S}\right)^2 + (3X_{lr})^2} \tag{21}$$

and

$$X_{3m} = \left(\frac{\Phi_{3m}}{\Phi_{1m}} \frac{F_{1m}}{F_{3m}}\right) X_m \tag{22}$$

Once again this result shows that X_{3m} reflects the degree of the main flux path saturation. It is thus a function of the main flux level.

Using typical per unit values for induction machines as shown in Table I, the relative magnitude and phase-shift of the resultant third harmonic flux are calculated for small, medium and large size machines, as shown in Fig. 9. Note from Fig. 9a that the majority of the no-load third harmonic flux remains despite of the reaction of the rotor third harmonic current at load. Also, it can be seen from Fig. 9b that a substantial phase-shift does exist between the resultant third harmonic flux and the no-load third harmonic flux, especially for large machines. The phase-shift decreases as the slip increases because the reactive component of the third harmonic current becomes dominant. It is interesting to note that the phase-shift of the resultant third harmonic flux tends to be negligible for small machines with smaller magnetizing inductances.

Table I Typical Per Unit Values of Induction Machine Parameters

hp	Xm	Xlr	r_r	Sn
3.0	1.0	0.08	0.10	0.10
15.0	2.0	0.10	0.05	0.05
100.0	5.0	0.15	0.01	0.01

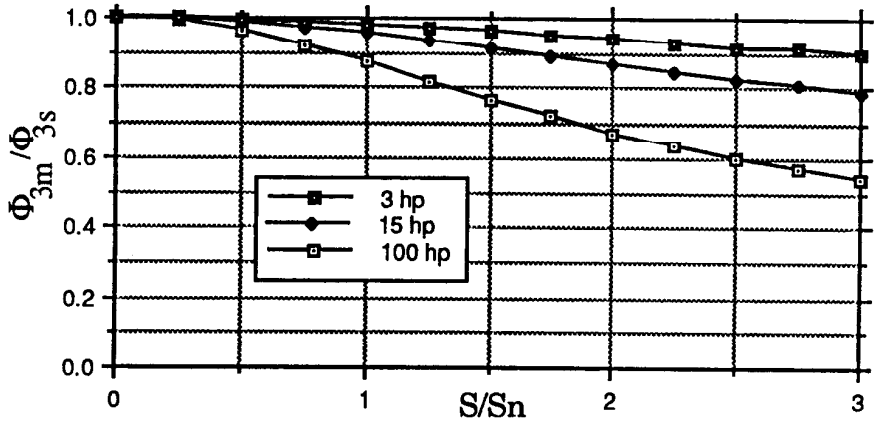

(a) Magnitude of the 3rd harmonic flux

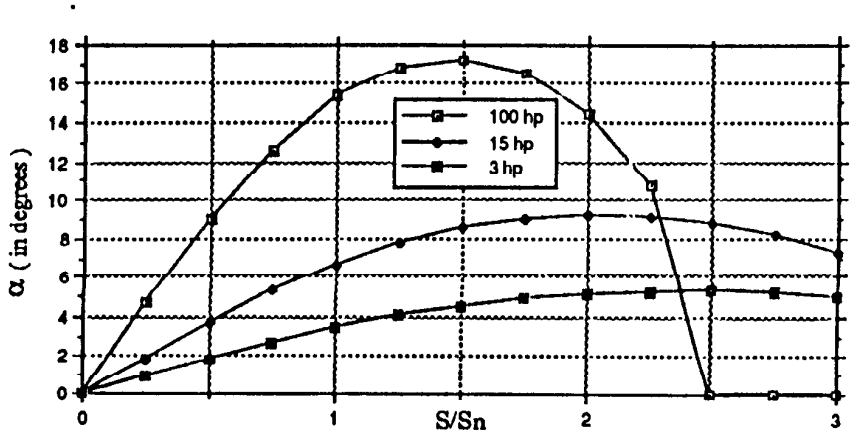

(b) Phase-shift of the 3rd harmonic flux

Fig. 9 Steady State Characteristics of Saturation Third Harmonic with Load

6. Modified Equivalent Circuit of Induction Machines Including the 3rd Harmonic Effect

Since the power transferred via the third harmonic airgap flux is reflected in the fundamental airgap flux by a change in the magnitude and phase-shift, this action can be viewed in terms of a fundamental component of current and voltage. A referral procedure is proposed in this section to link the rotor third harmonic circuit quantities to a set of equivalent fundamental circuit quantities as can be observed from the stator side. This referral is based on power transfer from the fundamental to the third harmonic.

The equations for the third harmonic torque and the third harmonic current can be re-arranged as follows:

$$T_{e3} = 3(\frac{P}{2})\frac{1}{2\sqrt{2}} m_r \Phi_{3m} I_{3r} \cos(\varphi_{3r})$$

$$= (\frac{P}{2})\frac{1}{2\sqrt{2}} m_r \Phi_{1m} I'_{3r} \cos(\varphi_{3r}) \qquad (23)$$

$$I'_{3r} = \frac{1}{(\frac{\Phi_{1m}}{3\Phi_{3m}})^2} \frac{\frac{1}{2\sqrt{2}} S\omega_e \Phi_{1m}}{\sqrt{R_r^2+(3S\omega_e L_{lr})^2}}$$

$$= \frac{\frac{1}{2\sqrt{2}} S\omega_e \Phi_{1m}}{\sqrt{R'^2_{3r}+(S\omega_e L'_{3r})^2}} \qquad (24)$$

with

$$R'_{3r} = (\frac{\Phi_{1m}}{3\Phi_{3m}})^2 R_r; \qquad L'_{3r} = 3(\frac{\Phi_{1m}}{3\Phi_{3m}})^2 L_{lr} \qquad (25)$$

It can now be imagined that there exists a fictitious rotor circuit with R'_{3r} and L'_{3r} as defined by Eqn. (25), connected in parallel with the usual rotor circuit, resulting in an additional rotor current produced by the airgap fundamental flux only. It can be shown that the rotor copper loss is invariant under the above referral. It is important to note that the referal factor $(\frac{\Phi_{1m}}{3\Phi_{3m}})^2$ includes all needed information about the third harmonic flux level and is thus a well defined function of L_{3m}, S, R_r, L_{lr}, as well as the main flux level. Note also that Φ_{3m} equals to Φ_{3s} approximately for small to medium size machines.

The above referal based on electromechanic power conversion enables a generalized treatment of torque production of the induction motor from the perspective of electromechanical energy conversion, as viewed from the stator side only. The result is a modified equivalent circuit for induction machines including the effect of the saturation third harmonic as shown in Fig. 10.

It is clear that when the main magnetic path is not saturated, ($\Phi_{1m}/3\Phi_{3m}$) tends to infinity. The modified equivalent circuit then reduces to the conven-tional equivalent circuit. With deep saturation, the current and the torque production of the third harmonic circuit is significant. This fact suggests that the satu-ration harmonic torque should be allowed for properly in an optimal design process and in the implementation of advanced control strategies for induction machines.

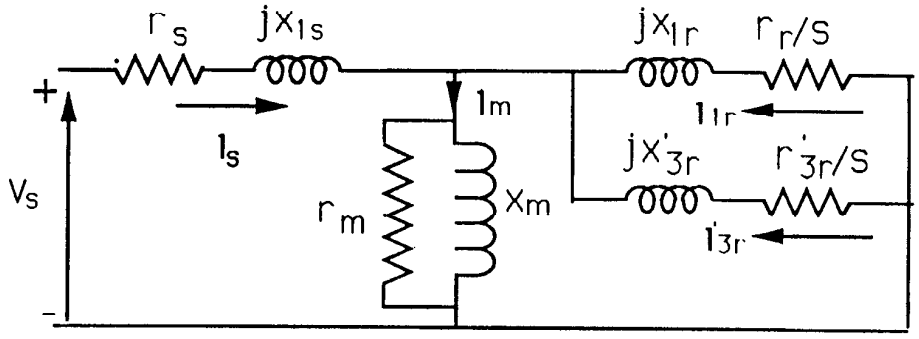

Fig. 9 Modified Equivalent Circuit for Induction Machines including the Effect of Third Harmonic

7. Conclusion

A detailed investigation of the effects of the third saturation harmonic on the performance of squirrel-cage induction machines has been made using a proposed simplified airgap field model. Based on this analysis, a modified equivalent circuit of induction machines including the third spatial saturation harmonic is proposed. This new model is believed to hold considerable promise for improved performance calculation.

Acknowledgement

The authors wish to acknowledge the support of the Wisconsin Electric Machine and Power Electronics Consortium (WEMPEC). Thanks are also due to Patrick Jansen of Dept. of ECE, UW-Madison for careful reading of the proof and valuable suggestions.

List of Principal Symbols

D_i : Bore diameter of the induction machine

l_{eff} : Effective bore length of the induction machine

ω_e : Synchronous angular speed

S : Slip ($S = S_1 = S_3$)

S_n : Rated slip

m_r : Number of rotor bars

w_s : Number of turns of the stator winding

k_w : Stator winding factor

p : Number of poles

R_r : Nominal value of the rotor resistance (per bar)

L_{1r} : Nominal value of the rotor leakage inductance (per bar)

r_s, r_r : Stator and rotor resistances (per unit value)

x_{1s}, x_{1r}: Stator and rotor leakage reactances (per unit value)

x_m : Magnetizing reactance (per unit value)

r_m : Magnetizing (shunt) resistance (per unit value)

R'_{3r} : Equivalent 3rd harmonic rotor resistance (per bar) as referred to the fundamental

L'_{3r} : Equivalent 3rd harmonic rotor leakage inductance as referred to the fundamental

r'_{3r} : Per unit equivalent 3rd harmonic rotor resistance

x'_{3r} : Per unit equivalent 3rd harmonic rotor leakage reactance

x_{3m} : Third harmonic magnetizing inductance (per unit value)

Φ_{1m} : Magnitude of the fundamental airgap flux vector

Φ_{3s} : Magnitude of the no-load third harmonic airgap flux vector

Φ_{3r} : Magnitude of the rotor third harmonic airgap flux vector

Φ_{3m} : Magnitude of the resultant third harmonic airgap flux vector

φ_{1r},φ_{3r}: Phase angles of the fundamental and the 3rd harmonic rotor currents

Appendix I

Details of the Induction Machine Used

25-horsepower 4-pole 3 phase induction motor operated at 506 volts with the following design constants:

D_o = outside diameter = 8.8 inches
D = stator bore = 5.5 inches
L = core length = 8.0 inches
g = air gap = 0.0259 inch
D_t = rotor inside diameter = 2.75 inches
magnetic shaft diameter = 2.75 inches
lamination: electrical grade, 26 gage
S_1 = stator number of teeth = 36
S_2 = rotor number of teeth = 45
stator winding: 13 turns per coil, 2 parallel Y
coil throw: 1 to 8
d-c resistance: 0.295 ohm per phase at 75 degrees centigrade
rotor winding: squirrel cage with 50% conductivity aluminum
end ring cross section: 0.8 square inch
rotor skew: 0.53 inch on rotor surface
stator and rotor slot details are shown in Figs. 1(A) and 1(B)

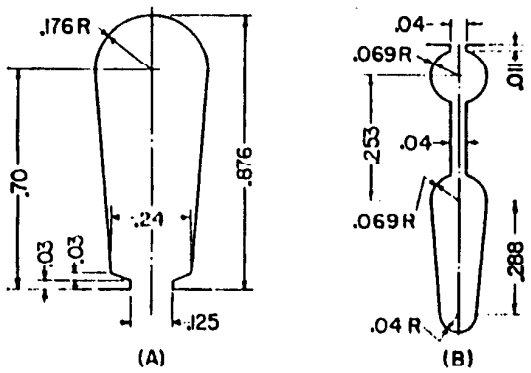

Fig. 1. Stator and rotor slot details

Appendix II

Derivation of Expressions (21-22) in Per Unit Value

Equation (20) can be expressed in terms of per unit values refered to the stator side by multiplying its numerator and denominator by $(\frac{k}{Z_b})^2$ where k is the stator to rotor turns and phase referal ratio defined by

$$k = \frac{4\, m_s\, (w_s\, k_w)^2}{m_r}$$

and Z_b the base impedance. One obtains

$$a = 1 + \frac{\left(\frac{k}{Z_b}\,\frac{1}{2\sqrt{2}}\,3\omega_e L_{3m}\right)^2}{\left(\frac{k}{Z_b}\,\frac{R_r}{S}\right)^2 + \left(\frac{k}{Z_b}\,3\omega_e L_{lr}\right)^2} = 1 + \frac{X_{3m}^2}{\left(\frac{r_r}{S}\right)^2 + (3X_{lr})^2} \qquad \text{(a.1)}$$

$$b = \frac{6X_{lr}X_{3m}}{(\frac{r_r}{S})^2+(3X_{lr})^2} \qquad \text{(a.2)}$$

To relate X_{3m} to the per unit magnetizing inductance resulting from the fundamental component of flux density, X_m, it can be recalled that for the fundamental component, if referred to the rotor side,

$$\frac{(Z_b\ X_m)\ I_m}{k} = E_{1r} = \frac{1}{2\sqrt{2}}\omega_e\Phi_{1m} \qquad \text{(a.3)}$$

Therefore,

$$X_m = \frac{k}{Z_b}\frac{1}{2\sqrt{2}}\omega_e\frac{\Phi_{1m}}{I_m}$$

$$= \frac{k}{Z_b}\ \frac{1}{2\sqrt{2}}\ \omega_e\frac{\Phi_{1m}}{F_{1m}}\ \frac{\sqrt{2}}{2\pi}\ \frac{m_r}{(\frac{p}{2})}$$

$$= \frac{k}{Z_b}\ \frac{1}{2\sqrt{2}}\ 3\omega_e\frac{\Phi_{1m}}{F_{1m}}\ \frac{\sqrt{2}}{2\pi}\ \frac{m_r}{3(\frac{p}{2})}$$

$$= \frac{\Phi_{1m}}{\Phi_{3m}}\ \frac{F_{3m}}{F_{1m}}\ [\frac{k}{Z_b}\ \frac{1}{2\sqrt{2}}\ 3\omega_e(\frac{\Phi_{3r}}{F_{3m}}\ \frac{\sqrt{2}}{2\pi}\ \frac{m_r}{3(\frac{p}{2})})]$$

$$= \frac{\Phi_{1m}}{F_{1m}}\ \frac{F_{3m}}{\Phi_{3m}}\ X_{3m} \qquad \text{(a.4)}$$

Hence

$$X_{3m} = \frac{\frac{\Phi_{3m}}{F_{3m}}}{\frac{\Phi_{1m}}{F_{1m}}}\ X_m \qquad \text{(a.5)}$$

References

[1] D. Kirschen, D. W. Novotny and T. A. Lipo,"On-Line Efficiency Optimization of a Variable Frequency Induction Motor Drive", *IEEE Trans. on Industry Applications*, vol. IA-21, May/June 1985, pp. 610-616.

[2] I.T. Wallace, D.W. Novotny, R.D. Lorenz, D.M. Divan,"Increasing the Torque Per Ampere Capability of Induction Machines", *IEEE IAS Annual Meeting*, 1991, pp. 14-20.

[3] C.H. Lee, "Saturation Harmonics of Polyphase Induction Machines", *Trans. AIEE*, vol. 80, Oct. 1961, pp. 597-603.

[4] B.J. Chalmers and R. Dodgson,"Waveshapes of Flux Density in Polyphase Induction Machines under Saturation Conditions", *IEEE Trans. on Power Apparatus and Systems*, Vol. 90, No. 2, March/April, 1971, pp. 564-569.

[5] J.C. Moreira and T.A. Lipo," Modelling of Saturated AC Machines Including Airgap Flux Harmonic Components", *Trans. 1990 IEEE Ind. Appl. Soc. Annual Meeting*, Oct. 1990, pp. 37-44.

[6] E. Levi and V. Vuckovic,"Field-Oriented Control of Induction Machines in the Presence of Magnetic Saturation", *Electric Machines and Power Systems*, Vol. 16, No.2 1989, pp.133-147.

[7] J.A.A. Melkebeek and D.W. Novotny,"The Influence of Saturation on Induction Machine Drive Dynamics", *IEEE Trans. on Ind. Appl.*, Vol. 19, No. 5, Sept/Oct, 1983, pp. 671-681.

[8] Y. He and T.A. Lipo,"Computer Simulation of an Induction Machine with Spatially Dependant Saturation", *IEEE Trans. on Power Apparatus and Systems*, Vol. 103, No. 4, April, 1984, pp. 707-714.

[9] P. Vas, K.E. Hallenius and J.E. Brown,"Cross Saturation in Smooth Air Gap Electrical Machines", *IEEE Trans. on Energy Conversion*, Vol. EC-1, pp. 103-112.